HAL
open science

Modelling and simulation of the nonlinear viscoelastic behavior of brain structures on complex domains

Maya de Buhan, Pascal Frey

To cite this version:

Maya de Buhan, Pascal Frey. Modelling and simulation of the nonlinear viscoelastic behavior of brain structures on complex domains. 2010. hal-00472813

HAL Id: hal-00472813

https://hal.science/hal-00472813v1

Preprint submitted on 13 Apr 2010

HAL is a multi-disciplinary open access archive for the deposit and dissemination of scientific research documents, whether they are published or not. The documents may come from teaching and research institutions in France or abroad, or from public or private research centers.

L'archive ouverte pluridisciplinaire **HAL**, est destinée au dépôt et à la diffusion de documents scientifiques de niveau recherche, publiés ou non, émanant des établissements d'enseignement et de recherche français ou étrangers, des laboratoires publics ou privés.

Modelling and simulation of the nonlinear viscoelastic behavior of brain structures on complex domains

M. de Buhan[a,b,*], P. Frey[a]

[a] *UPMC Univ Paris 06, UMR 7598, Laboratoire J.L. Lions, F-75005 Paris, France*
[b] *Universidad de Chile, FCFyM, Depto. de Ingeniería Matemática, Santiago, Chile*

Abstract

We consider the problem of modelling the deformation of cerebral structures for which the nonlinear viscoelastic behavior has been established several years ago by [9]. Based on the thorough mathematical analysis by [6] of a model with internal variable, we focus here on the implementation in three dimensions of a generalized version of this model. Computational results will be analyzed (i) to validate our model on toy problems wih simple geometries, for which pseudo analytical solutions are known and (ii) to emphasize the adaptation on the geometric properties of the boundaries for complex domains. These results are confronted to experimental results in order to assess the underlying model.

Keywords: nonlinear viscoelasticity, behavior of brain structure, finite element method, mesh adaptation
2000 MSC: 74B20, 35Q74, 65N50

1. Introduction

In this paper, we address the numerical aspects and the implementation of a mathematical model of nonlinear viscoelasticity in view of simulating the deformation of the brain structures, or more generally, of soft tissue. Indeed, in a clinical context, such deformations may occur consecutively to a change of position of the patient or during a neurosurgical treatment. Recent studies [9, 10, 1] tend to show that the amplitude of these deformations

*Maya de Buhan, *debuhan@ann.jussieu.fr*
This work has been supported by doctoral fellowships from CNRS and CONICYT.

is sufficiently large so that a model in large strains, *i.e* nonlinear, is fully acknowledged and that the brain material property is inherently viscoelastic. Health care expectations are related to the ability of such model to predict the centimeter-scale motion or shift [8] that occurs in surgery and thus to participate actively to the treatment planning of surgical operations.

Among the various types of models available, we have deliberately considered the model which introduces an additional internal variable governed by a differential equation in time, initially introduced by [13, 7] and mathematically analyzed in [6, 5]. We describe here the discretization and the implementation in three dimensions of a generalized version of this model, in a sense that will be made clear later, with the aim of obtaining the most accurate possible numerical results. To this end, we needed to solve this problem on triangulations especially adapted to the geometric shape complexity of the computational domains at hand, defined from discrete imaging data. Numerical results will be assessed through experimental results in order to validate the underlying model and to fit at best the relevant biophysical coefficients.

This work can be considered as a preliminary, but nevertheless an essential stage of a broader study in which this model will be coupled with a fluid model and/or with a viscoplastic model, most likely suitable for representing the behavior of brain structures. Furthermore, the accurate resolution of the direct problem is needed in the study of related inverse problems which purpose is to retrieve the biophysical coefficients of the model, in the case where no experimental or reliable data are available.

1.1. The generalized model

At first, we present the viscoelastic model in large strains that we used in numerical simulations and we explain how our version differs and generalizes the classical model [13].

Let Ω be a connected and bounded open set of $\mathbb{R}^3$ corresponding to the reference configuration. We suppose that the boundary Γ of Ω is Lipschitz-continuous, thus the outer unit normal vector n is well defined at each boundary point. We assume also that the boundary can be decomposed as $\Gamma = \Gamma_0 \cup \Gamma_1$ with $\Gamma_0 \cap \Gamma_1 = \emptyset$. The model problem we consider is the following:

Find the displacement vector u solving:

$$\begin{cases} -\text{div } T = f, & \text{in } \Omega, \\ u = 0, & \text{on } \Gamma_0, \\ T \cdot n = g, & \text{on } \Gamma_1, \end{cases}$$

where f (resp. g) represents the body (resp. surface) forces, expressed in the reference configuration. The constitutive law is then given by the following relation, that relate the first Piola-Kirchhoff stress tensor T to the gradient of deformation $F = Id + \nabla u$:

$$T = \frac{dW}{dF} - pF^{-T}. \tag{1}$$

In the viscoelastic model we consider here, the elastic energy W of the system can be written as follows:

$$W(C, G_1, G_2) = W_0(C) + W_1(C : G_1) + W_2(C : G_2), \tag{2}$$

where the Cauchy-Green strain tensor C is defined as:

$$C = F^T F = Id + \nabla u + \nabla u^T + \nabla u \cdot \nabla u^T,$$

and where the tensors G_1 and G_2 are two internal variables used to measure the deformation of two dashpots embedded in the material. The evolution of these internal variables is described by the set of following equations:

$$\begin{cases} \nu_i \dot{G}_i^{-1} = \dfrac{\partial W}{\partial G_i} + q_i G_i^{-1}, & \text{in } \Omega, \\ G_i(0) = Id, & \text{in } \Omega, \end{cases} \qquad \forall i \in \{1, 2\}, \tag{3}$$

with ν_1 and ν_2 the viscosity coefficients. The pressures p, q_1 and q_2 occuring in equations (1) and (3) are the Lagrange multipliers associated to the incompressibility constraints:

$$\det(F) = \det(G_1) = \det(G_2) = 1.$$

At this point, we observe that this model is slightly different from the model described in [6], in the sense that it contains a supplementary internal variable, hereby justifying its denomination of generalized model. In other words, if the model of [6] is a nonlinear version of the Maxwell model, by analogy our

model can be seen as a nonlinear version of the generalized Maxwell model. This rather complex formulation is indeed required by the application we have in mind, as will be emphasized in the numerical examples presented in Section 3.

In view of its numerical resolution using the finite element method, a weak formulation of this problem shall be first written, which leads now to solve: Find $u \in \mathcal{V}$, $p \in \mathcal{P}$, $G_i \in \mathcal{H}$ and $q_i \in \mathcal{Q}$, for $i \in \{1, 2\}$, such that:

$$\begin{cases} \displaystyle\int_\Omega \left(2F\frac{\partial W}{\partial C}(C, G_1, G_2) - pF^{-T}\right) : \nabla v \, dx \\ \qquad\qquad \displaystyle= \int_\Omega f \cdot v \, dx + \int_{\Gamma_1} g \cdot v \, d\gamma, & \forall v \in \mathcal{V}, \\ \displaystyle\int_\Omega \hat{p} \left(\det(F) - 1\right) dx = 0, & \forall \hat{p} \in \mathcal{P}, \\ \displaystyle\int_\Omega \left(-\frac{\partial W_i}{\partial y}(C : G_i)C + \nu_i \dot{G}_i^{-1} - q_i G_i^{-1}\right) : H \, dx = 0, & \forall H \in \mathcal{H}, \\ \displaystyle\int_\Omega \hat{q} \left(\det(G_i) - 1\right) dx = 0, \quad \forall i \in \{1, 2\}, & \forall \hat{q} \in \mathcal{Q}, \end{cases} \tag{4}$$

where the functional spaces are chosen accordingly, *i.e.* such that all integrals are well defined, and : denotes the double contraction of tensors. Furthermore, the energy function defined in (2) leads to write:

$$\frac{\partial W}{\partial C}(C, G_1, G_2) = \frac{\partial W_0}{\partial C}(C) + \frac{\partial W_1}{\partial y}(C : G_1)G_1 + \frac{\partial W_2}{\partial y}(C : G_2)G_2.$$

Thus, the problem associates a nonlinear PDE endowed with an incompressibility condition and two ODE describing the time evolution of the internal variables.

1.2. Paper outline

This remainder of this paper is divided in two parts. The first part describes the discretization stage and the numerical resolution of the mechanical model. The second part concerns two examples of numerical simulations in complex geometries and is aimed at outlining the efficiency of our approach.

2. Numerical approximation

In this part, following the outline of the paper [6], we explain the main stages of the discretization of our model and the resolution techniques that

have been effectively implemented in this study. The spatial discretization involves $\mathbb{P}_0/\mathbb{P}_2$ Lagrange finite elements and the time discretization is based on an implicit Euler scheme. The linearized version of the resulting system derives naturally from a Newton method and is solved using an Augmented Lagrangian technique.

2.1. Space discretization

Hereafter, we consider a conforming triangulation $\mathcal{T}_h$ of the computational domain Ω where h represents the characteristic mesh size. The variational approximation of the initial problem (4) is classically obtained by replacing the functional spaces $\mathcal{V}$, $\mathcal{P}$, $\mathcal{H}$ and $\mathcal{Q}$ by finite dimensional subspaces $\mathcal{V}_h$, $\mathcal{P}_h$, $\mathcal{H}_h$ and $\mathcal{Q}_h$, respectively. We are well aware that the choice of these spaces is of importance to ensure the stability of the resolution. An analysis stage must confirm the validity of this choice, although it is out of the scope of this paper. Namely, we have retained the following finite elements spaces:

$$\begin{aligned}
\mathcal{V}_h &= \left\{ v_h : \overline{\Omega} \longrightarrow \mathbb{R}^3,\ \forall K \in \mathcal{T}_h,\ v_h|_K \in \mathbb{P}_2^3,\ v_h = 0 \text{ on } \Gamma_0 \right\}, \\
\mathcal{P}_h &= \mathcal{Q}_h = \left\{ p_h : \overline{\Omega} \longrightarrow \mathbb{R},\ \forall K \in \mathcal{T}_h,\ p_h|_K \in \mathbb{P}_0 \right\}, \\
\mathcal{H}_h &= \left\{ H_h : \overline{\Omega} \longrightarrow \mathcal{U},\ \forall K \in \mathcal{T}_h,\ H_h|_K \in \mathbb{P}_0^5 \right\}.
\end{aligned}$$

where $\mathcal{U} = \{H \in (\mathcal{M}_3)_{sym}, \det(H) = 1\}$. Consequently, the problem (4) becomes:
Find $u_h \in \mathcal{V}_h$, $p_h \in \mathcal{P}_h$, $G_{ih} \in \mathcal{H}_h$ and $q_{ih} \in \mathcal{Q}_h$, for $i \in \{1, 2\}$, such that:

$$\begin{cases}
\displaystyle\int_\Omega \left(2F_h \frac{\partial W}{\partial C}(C_h, G_{1h}, G_{2h}) - p_h F_h^{-T} \right) : \nabla v_h \, dx \\
\qquad\qquad \displaystyle= \int_\Omega f \cdot v_h \, dx + \int_{\Gamma_1} g \cdot v_h \, d\gamma, & \forall v_h \in \mathcal{V}_h, \\
\displaystyle\int_\Omega \hat{p}_h (\det(F_h) - 1) \, dx = 0, & \forall \hat{p}_h \in \mathcal{P}_h, \\
\displaystyle\int_\Omega \left(-\frac{\partial W_i}{\partial y}(C_h : G_{ih}) C_h + \nu_i \dot{G}_{ih}^{-1} - q_{ih} G_{ih}^{-1} \right) : H_h \, dx = 0, & \forall H_h \in \mathcal{H}_h, \\
\displaystyle\int_\Omega \hat{q}_h (\det(G_{ih}) - 1) \, dx = 0, & \forall i \in \{1, 2\}, \quad \forall \hat{q}_h \in \mathcal{Q}_h.
\end{cases}$$

As $\mathcal{H}_h$ and $\mathcal{Q}_h$ are spaces composed of piecewise constant functions, the last equations can be further simplified as:

$$\begin{cases} -\dfrac{\partial W_i}{\partial y}(C_h : G_{ih})C_h + \nu_i \dot{G}_{ih}^{-1} - q_{ih}G_{ih}^{-1} = 0, & \text{in each } K \in \mathcal{T}_h, \\ \det(G_{ih}) = 1, \qquad \forall i \in \{1,2\}, & \text{in each } K \in \mathcal{T}_h. \end{cases}$$

2.2. Time discretization

We focus now on the time discretization of the problem using an implicit Euler scheme, which is unconditionnally stable. This is an essential requisite for dealing with the various time scales occuring in viscoelastic phenomena. Let Δt be the time discretization step. The numerical scheme we considered leads to solve the following sequence of problems:
For $n \in \mathbb{N}$, find $u_h^{n+1} \in \mathcal{V}_h$, $p_h^{n+1} \in \mathcal{P}_h$, $G_{ih}^{n+1} \in \mathcal{H}_h$ and $q_{ih}^{n+1} \in \mathcal{Q}_h$ solving:

$$\begin{cases} \displaystyle\int_\Omega \left(2F_h^{n+1}\frac{\partial W}{\partial C}(C_h^{n+1}, G_{1h}^{n+1}, G_{2h}^{n+1}) - p_h^{n+1}(F_h^{n+1})^{-T} \right) : \nabla v_h \, dx \\ \qquad\qquad = \displaystyle\int_\Omega f \cdot v_h \, dx + \int_{\Gamma_1} g \cdot v_h \, d\gamma, \qquad \forall v_h \in \mathcal{V}_h, \\ \displaystyle\int_\Omega \hat{p}_h(\det(F_h^{n+1}) - 1) \, dx = 0, \qquad \forall \hat{p}_h \in \mathcal{P}_h, \\ \nu_i \dfrac{(G_{ih}^{n+1})^{-1} - (G_{ih}^{n})^{-1}}{\Delta t} - \dfrac{\partial W_i}{\partial y}(C_h^{n+1} : G_{ih}^{n+1})C_h^{n+1} - q_{ih}^{n+1}(G_{ih}^{n+1})^{-1} = 0, \\ \det(G_{ih}^{n+1}) = 1, \qquad \forall i \in \{1,2\}, \quad \text{in each } K \in \mathcal{T}_h, \end{cases}$$

endowed with the initial condition $G_{ih}^0 = Id$. The numerical resolution of this tedious problem is carried out in two steps. At first, we solve the evolution equations of the internal variables and express the latter in terms of the unknown C_h^{n+1}. As the resulting problem depends only on C_h^{n+1}, it can then be solved as a classical nonlinear elastic problem.

2.3. Calculation of the viscoelastic variables

At each time step, we can compute each one of the two viscoelastic variables G_{ih}^{n+1}, $\forall i \in \{1,2\}$, independently, by solving its evolution equation in each element K in $\mathcal{T}_h$. To this end, we observe first that the problem can be rewritten, for each time step $n \in \mathbb{N}$, as the following minimization problem:

$$G_{ih}^{n+1} = \arg\min_{H \in \mathcal{U}} \left(W_i(C_h^{n+1} : H) + \frac{\nu_i}{\Delta t}(G_{ih}^n)^{-1} : H \right), \quad \forall i \in \{1,2\}.$$

Then, we consider G_i as a function defined on $\mathbb{R}^5$ with value in $\mathcal{U}$ of the form:

$$\begin{aligned} G_i(Z) =& Z_1(e_1 \otimes e_1) + Z_4(e_2 \otimes e_2) + Z_2(e_1 \otimes e_2 + e_2 \otimes e_1) \\ &+ Z_3(e_1 \otimes e_3 + e_3 \otimes e_1) + Z_5(e_2 \otimes e_3 + e_3 \otimes e_2) \\ &+ \frac{1 + Z_1 Z_5^2 + Z_4 Z_3^2 - 2 Z_2 Z_3 Z_5}{Z_1 Z_4 - Z_2^2}(e_3 \otimes e_3), \end{aligned}$$

where $\otimes$ denotes the tensor product and we defined $Y_i \in \mathbb{R}^5$ such that $G_i(Y_i) = G_{ih}^{n+1}$, for $i \in \{1, 2\}$.
Thus, the minimization problem reads now:

$$Y_i = \arg\min_{Z \in \mathbb{R}^5} \left(W_i(C_h^{n+1} : G_i(Z)) + \frac{\nu_i}{\Delta t}(G_{ih}^n)^{-1} : G_i(Z) \right),$$

that is also equivalent to:

$$\mathcal{F}_i(Y_i, C_h^{n+1}) = 0, \qquad \forall i \in \{1, 2\}, \tag{5}$$

where the function $\mathcal{F}_i$ is defined, for all $(Z, C) \in \mathbb{R}^5 \times \mathcal{U}$ by:

$$\mathcal{F}_i(Z, C) = \left(\frac{\partial W_i}{\partial y}(C : G_i(Z))C + \frac{\nu_i}{\Delta t}(G_{ih}^n)^{-1} \right) : \frac{\partial G_i}{\partial Z}(Z).$$

Next, we observe that the nonlinear equation (5) defines an implicit function $Y_i = \mathcal{Y}_i(C_h^{n+1})$ that can be easily computed using a classical Newton method on $\mathbb{R}^5$. At each iteration, the linear operator that needs to be inverted is given by:

$$\begin{aligned} K_i = \frac{\partial \mathcal{F}_i}{\partial Z}(Z, C) =& \frac{\partial^2 W_i}{\partial y^2}(C : G_i(Z))(C : \frac{\partial G_i}{\partial Z}(Z)) \otimes (C : \frac{\partial G_i}{\partial Z}(Z)) \\ &+ \left(\frac{\partial W_i}{\partial y}(C : G_i(Z))C + \frac{\nu_i}{\Delta t}(G_{ih}^n)^{-1} \right) : \frac{\partial^2 G_i}{\partial Z^2}(Z). \end{aligned}$$

2.4. Resolution of the elastic problem

According to the relation $G_{ih}^{n+1} = G_i(\mathcal{Y}_i(C_h^{n+1})) = \mathcal{G}_i(C_h^{n+1})$, $\forall i \in \{1, 2\}$, we can replace the viscoelastic variables in the original problem (4) that becomes now:

Find $u_h^{n+1} \in \mathcal{V}_h$ and $p_h^{n+1} \in \mathcal{P}_h$ solving:

$$\begin{cases} \displaystyle\int_\Omega \left(2F_h^{n+1} \frac{\partial W}{\partial C}(C_h^{n+1}, \mathcal{G}_1(C_h^{n+1}), \mathcal{G}_2(C_h^{n+1})) - p_h^{n+1}(F_h^{n+1})^{-T} \right) : \nabla v_h \, dx \\ \qquad\qquad = \displaystyle\int_\Omega f \cdot v_h \, dx + \int_{\Gamma_1} g \cdot v_h \, d\gamma, \qquad\qquad \forall v_h \in \mathcal{V}_h, \\ \displaystyle\int_\Omega \hat{p}_h (\det(F_h^{n+1}) - 1) \, dx = 0, \qquad\qquad \forall \hat{p}_h \in \mathcal{P}_h. \end{cases}$$

Let $(\phi_i)_{i=1..N}$ be a basis of $\mathcal{V}_h$ and $(\psi_i)_{i=1..M}$ be a basis of $\mathcal{P}_h$, respectively. If we consider the vector U_h^{n+1} (resp. P_h^{n+1}) of the components of u_h^{n+1} (resp. p_h^{n+1}) in the basis $(\phi_i)_{i=1..N}$ (resp. $(\psi_i)_{i=1..M}$), our finite element problem takes, at each time step n, the form of an algebraic system of $N+M$ nonlinear equations with $N+M$ unknowns:
Find $(U_h^{n+1}, P_h^{n+1}) \in \mathbb{R}^N \times \mathbb{R}^M$ such that:

$$\mathcal{L}(U_h^{n+1}, P_h^{n+1}) = 0, \qquad \text{in } \mathbb{R}^N \times \mathbb{R}^M,$$

with the notations, for all $(U, P) \in \mathbb{R}^N \times \mathbb{R}^M$:

$$\begin{aligned} \mathcal{L}_j(U,P) &= \int_\Omega 2F \frac{\partial W}{\partial C}(C, \mathcal{G}_1(C), \mathcal{G}_2(C)) : \nabla \phi_j \, dx - \int_\Omega pF^{-T} : \nabla \phi_j \, dx \\ &\quad - \int_\Omega f \cdot \phi_j \, dx - \int_{\Gamma_1} g \cdot \phi_j \, d\gamma, \qquad\qquad \forall j \in \{1..N\}, \\ \mathcal{L}_{j+N}(U,P) &= - \int_\Omega \psi_j (\det(F) - 1) dx, \qquad\qquad \forall j \in \{1..M\}. \end{aligned}$$

This system can be very large but sparse. It can be easily linearized by a Newton algorithm.

2.5. Linearization by a Newton method

To solve the nonlinear equation $\mathcal{L}(U_h^{n+1}, P_h^{n+1}) = 0$ using Newton's method, we have to compute the gradient matrix $\dfrac{D\mathcal{L}}{D(U,P)}$ that is defined for all

$(U, P, V, Q) \in \mathbb{R}^N \times \mathbb{R}^M \times \mathbb{R}^N \times \mathbb{R}^M$ by:

$$\begin{aligned}
\frac{\partial \mathcal{L}_j}{\partial U}(U,P)V = &\int_\Omega \left(4\frac{d}{dC}\left(\frac{\partial W}{\partial C}(C, \mathcal{G}_1(C), \mathcal{G}_2(C))\right) : F^T\nabla v\right) : F^T\nabla\phi_j\, dx \\
&+ \int_\Omega 2\frac{\partial W}{\partial C}(C, \mathcal{G}_1(C), \mathcal{G}_2(C)) : \nabla v^T \nabla\phi_j\, dx \\
&- \int_\Omega p\left(\frac{\partial (F^{-T})}{\partial F} : \nabla v\right) : \nabla\phi_j\, dx, \qquad \forall j \in \{1..N\}, \\
\frac{\partial \mathcal{L}_{j+N}}{\partial U}(U,P)V = &- \int_\Omega \psi_j F^{-T} : \nabla v\, dx, \qquad \forall j \in \{1..M\}, \\
\frac{\partial \mathcal{L}_j}{\partial P}(U,P)Q = &- \int_\Omega q F^{-T} : \nabla\phi_j\, dx, \qquad \forall j \in \{1..N\}, \\
\frac{\partial \mathcal{L}_{j+N}}{\partial P}(U,P)Q = &0, \qquad \forall j \in \{1..M\}.
\end{aligned}$$

We notice that the differential $\frac{d}{dC}\left(\frac{\partial W}{\partial C}(C, \mathcal{G}_1(C), \mathcal{G}_2(C))\right)$ must be computed, which implies knowing the derivatives $\partial\mathcal{G}_i/\partial C$, $\forall i \in \{1,2\}$. The implicit function theorem states that:

$$\begin{aligned}
&\mathcal{F}_i(Y_i, C_h^{n+1}) = 0 \qquad \Longleftrightarrow \qquad Y_i = \mathcal{Y}_i(C_h^{n+1}) \qquad \text{and} \\
&\frac{\partial \mathcal{Y}_i}{\partial C}(C_h^{n+1}) = -\left(\frac{\partial \mathcal{F}_i}{\partial Z}(\mathcal{Y}_i(C_h^{n+1}), C_h^{n+1})\right)^{-1} \cdot \left(\frac{\partial \mathcal{F}_i}{\partial C}(\mathcal{Y}_i(C_h^{n+1}), C_h^{n+1})\right)^T,
\end{aligned}$$

and allows us to find the differential as follows:

$$\begin{aligned}
&\frac{d}{dC}\left(\frac{\partial W}{\partial C}\,(C, \mathcal{G}_1(C), \mathcal{G}_2(C))\right) = \frac{\partial^2 W_0}{\partial C^2}(C) - B_1 \cdot K_1^{-1} \cdot B_1^T - B_2 \cdot K_2^{-1} \cdot B_2^T \\
&+ \frac{\partial^2 W_1}{\partial y^2}(\mathcal{G}_1(C) : C)(\mathcal{G}_1(C) \otimes \mathcal{G}_1(C)) + \frac{\partial^2 W_2}{\partial y^2}(\mathcal{G}_2(C) : C)(\mathcal{G}_2(C) \otimes \mathcal{G}_2(C)),
\end{aligned}$$

with, for $i \in \{1,2\}$:

$$\begin{aligned}
B_i &= \frac{\partial \mathcal{F}_i}{\partial C}(\mathcal{Y}_i(C), C) \\
&= \frac{\partial^2 W_i}{\partial y^2}(C : \mathcal{G}_i(C))\mathcal{G}_i(C) \otimes (C : \frac{\partial G_i}{\partial Z}(\mathcal{Y}_i(C))) + \frac{\partial W_i}{\partial y}(C : \mathcal{G}_i(C))\frac{\partial G_i}{\partial Z}(\mathcal{Y}_i(C)).
\end{aligned}$$

Remark. It is well known that the Newton method is very sensitive to its intialization and may not converge in some cases, *i.e.* if the initial data differs largely from the solution. To overcome this drawback, the classical initialization strategy consists in using an incremental loading [12]. In this technique, the load acting on the body is applied as small increments. The equilibrium position is then computed at the end of each load increment using as initial guess the position obtained at the previous increment.

2.6. General algorithm

In this section, we summarize the main successive stages for solving the viscoelastic problem in large strains.
We initialize U to the zero vector and P to the hydrostatic pressure at rest. We set $\lambda = 0$ and we increase it iteratively by a small increment $\Delta\lambda$ until the value $\lambda = 1$ is attained. For each load $(\lambda f, \lambda g)$, we compute the solution (U, P) by a Newton algorithm as follows:

1. Initialization
   We set (U_0, P_0) equal to the solution at the previous loading step and we compute the residual:
   $$R_0 = \mathcal{L}(U_0, P_0).$$
2. Iteration loop
   Then, for each $k \geq 0$, knowing U_k, P_k and R_k, we obtain U_{k+1}, P_{k+1} and R_{k+1} by:
   a) computing the gradient matrix:
   $$M_k = \frac{D\mathcal{L}}{D(U,P)}(U_k, P_k),$$
   b) solving the linear system:
   $$M_k(\Delta U, \Delta P) = -R_k, \tag{6}$$
   c) updating:
   $$(U_{k+1}, P_{k+1}) = (U_k, P_k) + (\Delta U, \Delta P),$$
   d) solving the two minimization problems on the viscoelastic variables using Newton loops to obtain $\mathcal{G}_i(C_k)$, $\forall i \in 1, 2$,
   e) evaluating the new residual:
   $$R_{k+1} = \mathcal{L}(U_{k+1}, P_{k+1}).$$

Remark. The linear system (6) to solve at each iteration of the Newton method can be solved by an augmented Lagrangian technique [11]. This iterative procedure consists in replacing at each iteration step the initial linear system by a simplest system that can be solved using a preconditionned conjugate gradient.

2.7. Validation

The aim of this section is to assess the numerical method by evaluating the discrepancy between the approximate solution and a pseudo analytical solution, *i.e.* the exact solution in space approximated in time using a finite difference scheme. To this end, we considered the simplest case for which a pseudo analytical solution can be computed, the compression of a cube fixed on one of its side. Indeed, in such test case, there is no relevant geometric issue.

We describe hereafter the computation of this solution on the reference cube. Let h_0 be the initial height of the sample and δ be its constant vertical elongation with respect to the Z-axis. We introduce the ratio:

$$\alpha = \frac{h_0 + \delta}{h_0} = 1 + \frac{\delta}{h_0}.$$

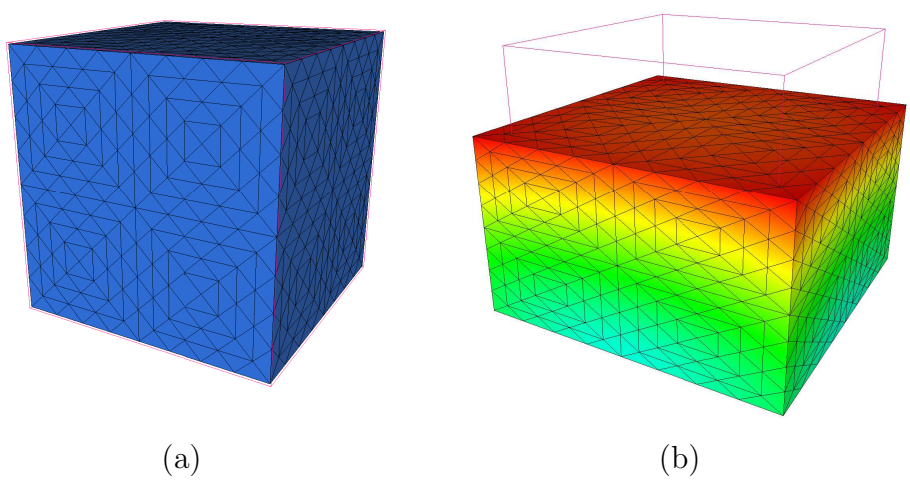

(a) (b)

Figure 1: (a) Configuration at rest, (b) Deformed configuration

Hence, we can define the transformation between the reference configuration (with respect to the variables X, Y, Z) and the deformed configuration (with respect to the variables x, y, z) by:

$$x = \gamma X, \qquad y = \gamma Y, \qquad z = \alpha Z,$$

where γ is the currently unknown horizontal dilatation coefficient, identical in X and Y thanks to the symmetry of the problem. We can then compute the displacement vector u, the gradient of deformation F and the strain tensor C, respectively, as follows:

$$u = \begin{pmatrix} (\gamma-1)X \\ (\gamma-1)Y \\ (\alpha-1)Z \end{pmatrix} \implies F = \begin{pmatrix} \gamma & 0 & 0 \\ 0 & \gamma & 0 \\ 0 & 0 & \alpha \end{pmatrix} \implies C = \begin{pmatrix} \gamma^2 & 0 & 0 \\ 0 & \gamma^2 & 0 \\ 0 & 0 & \alpha^2 \end{pmatrix},$$

and thanks to the incompressibility condition $\det(C) = 1$, we can deduce:

$$\gamma = \frac{1}{\sqrt{\alpha}},$$

yielding finally to:

$$C = \begin{pmatrix} 1/\alpha & 0 & 0 \\ 0 & 1/\alpha & 0 \\ 0 & 0 & \alpha^2 \end{pmatrix}.$$

The energy function is chosen as a Moonley-Rivlin energy functional:

$$\begin{aligned} W_0(C) &= \mathcal{C}_{01}(I_1(C) - 3) + \mathcal{C}_{02}(I_2(C) - 3), \\ W_i(y) &= \mathcal{C}_i(y - 3), \qquad \forall i \in \{1, 2\}. \end{aligned}$$

where $I_1(C) = \mathrm{tr}(C)$ and $I_2(C) = \frac{1}{2}\left((\mathrm{tr}(C))^2 - \mathrm{tr}(C^2)\right)$ are the first and second invariants of C and $\mathcal{C}_{01}$, $\mathcal{C}_{02}$ and $\mathcal{C}_i$ are constant coefficients in Pa. We need to compute the viscoelastic variables G_i in view of evalutating the stress tensor T. Each variable G_i, $\forall i \in \{1, 2\}$ satisfies the following ODE:

$$\nu_i \dot{G_i^{-1}} - q_i G_i^{-1} = \frac{\partial W_i}{\partial y}(C : G_i)C = \mathcal{C}_i C, \qquad \forall i \in \{1, 2\},$$

with $G_i(0) = Id$. This equation is discretized using the classical implicit finite differences scheme:

$$\nu_i \frac{(G_i^{n+1})^{-1} - (G_i^n)^{-1}}{\Delta t} - q_i^{n+1}(G_i^{n+1})^{-1} = \mathcal{C}_i C^{n+1},$$

thus leading to:

$$(G_i^{n+1})^{-1} = \frac{\frac{\nu_i}{\Delta t}(G_i^n)^{-1} + \mathcal{C}_i C^{n+1}}{\frac{\nu}{\Delta t} - q_i^{n+1}}, \qquad \forall i \in \{1,2\}. \tag{7}$$

Here, the unknown variable q_i^{n+1} can be determined using the incompressibility condition $\det((G_i^{n+1})^{-1}) = 1$ to obtain:

$$q_i^{n+1} = \frac{\nu_i}{\Delta t} - \left(\frac{\nu_i}{\Delta t}(G_i^n)^{-1} + \frac{\mathcal{C}_i}{\alpha}\right)^{2/3} \left(\frac{\nu}{\Delta t}(G_i^n)^{-1} + \mathcal{C}_i\alpha^2\right)^{1/3},$$

that depends only on the time step n (since α is constant) and can be replaced in (7). At this stage, we can compute the stress tensor T using (1):

$$\begin{aligned} T &= 2F\frac{\partial W}{\partial C}(C, G_1, G_2) - pF^{-T} \\ &= 2F\left(\mathcal{C}_{01} + \mathcal{C}_{02}(\mathrm{tr}(C)I - C) + \mathcal{C}_1 G_1 + \mathcal{C}_2 G_2\right) - pF^{-T}. \end{aligned}$$

Hence, the principal components of the diagonal tensor T can be expressed with respect to the elongation α as:

$$T_X = T_Y = \frac{2}{\sqrt{\alpha}}\left(\mathcal{C}_{01} + \mathcal{C}_{02}(\alpha^2 + \frac{1}{\alpha}) + \mathcal{C}_1(G_1)_X + \mathcal{C}_2(G_2)_X\right) - \sqrt{\alpha}p,$$

$$T_Z = 2\alpha\left(\mathcal{C}_{01} + \frac{2}{\alpha}\mathcal{C}_{02} + \mathcal{C}_1(G_1)_Z + \mathcal{C}_2(G_2)_Z\right) - \frac{p}{\alpha}.$$

By noticing that $T_X = T_Y = 0$, since the cube is not subjected to any load on the lateral sides, the pressure p can be determined:

$$p = \frac{2}{\alpha}\left(\mathcal{C}_{01} + \mathcal{C}_{02}(\alpha^2 + \frac{1}{\alpha}) + \mathcal{C}_1(G_1)_X + \mathcal{C}_2(G_2)_X\right).$$

It remains then to compute the non null vertical constraint T_Z as follows:

$$\begin{aligned} T_Z =& 2\left(\alpha\mathcal{C}_{01} + \mathcal{C}_{02}\right)\left(1 - \frac{1}{\alpha^3}\right) + 2\mathcal{C}_1\alpha\left((G_1)_Z - \frac{1}{\alpha^3}(G_1)_X\right) \\ &+ 2\mathcal{C}_2\alpha\left((G_2)_Z - \frac{1}{\alpha^3}(G_2)_X\right). \end{aligned}$$

As such, the pressure and the vertical constraint are both independent in space but need the computation of G_i, $\forall i \in \{1, 2\}$ to be estimated in time.

Now, we present the numerical result we obtained for this test case (for $\alpha = 0.7$). Table 1 reports the mechanical properties of our model. Figure 2 illustrates the time evolution of the pressure and the vertical constraint corresponding to the numerical and the pseudo analytical solutions.

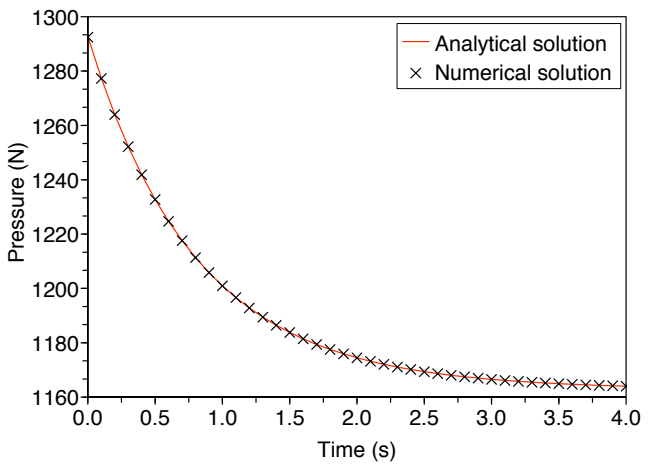

(a)

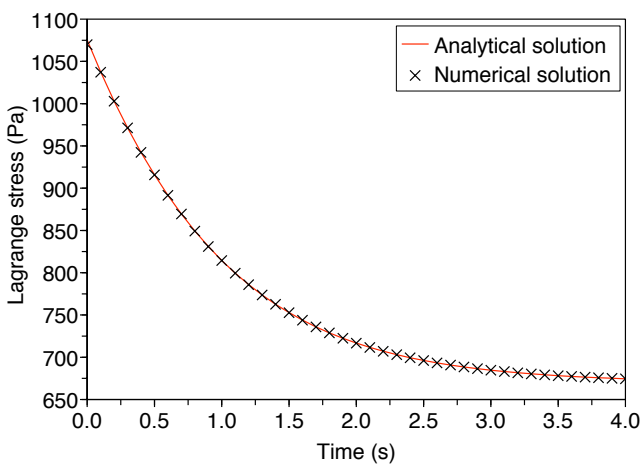

(b)

Figure 2: Evolution of the pressure (a) and the vertical stress (b) with respect to time during the compression test. Comparison between the pseudo analytical solution (continuous line) and the numerical solution (crosses).

Remark. In all examples, we have checked numerically (on the computational triangulation) that the total volume remains constant throughout the

compression stage, in compliance with the incompressibility condition of the model.

$\mathcal{C}_{01}$	$\mathcal{C}_{10}$	$\mathcal{C}_1$	ν_1	$\mathcal{C}_2$	ν_2
21	105	80	21500	150	115

Table 1: Mechanical properties used for the test case

3. Examples

In this section, we consider two application examples to illustrate other features of our approach. In the first example, we show the ability of dealing with the complex 3D geometry of a mechanical device. The second example is related to a biomedical application, the analysis of the brain shift. The aim of this example is twofold. Firstly, it shows that the generalized formulation of our model (see Section 1) is well suited to represent at best the physical behavior of the brain structure. Secondly, it emphasizes the need to develop an ad-hoc procedure to deal with the discrete data supplied by imaging devices.

3.1. Mechanical device

Figure 3 shows an example of a mechanical device corresponding to the domain $\Omega \subset 20 \times 20 \times 5$ cm, on which we applied a load $f = (50, 50, 50)$ $N \cdot m^{-3}$, while maintaining fixed two branches on the (O, x, z) plane. The maximal deformation is about 10 cm, obtained using the values reported in Table 1. The computational mesh contains $7,402$ vertices and $32,977$ tetrahedra. The inital volume is $8.761 \cdot 10^2$ cm^3 and the final volume after deformation is $8.760 \cdot 10^2$ cm^3.

3.2. Brain shift simulation

Next, we turn to a more realistic problem associated with the biomedical application we had in mind when starting this study, *i.e.,* the deformation of cerebral structures. In this complex problem, two aspects are of interest and need to be carefully addressed: (i) the fitting of biophysical parameters, based on experimental data and (ii) the accurate discretization of the computational domain, defined from imaging data.

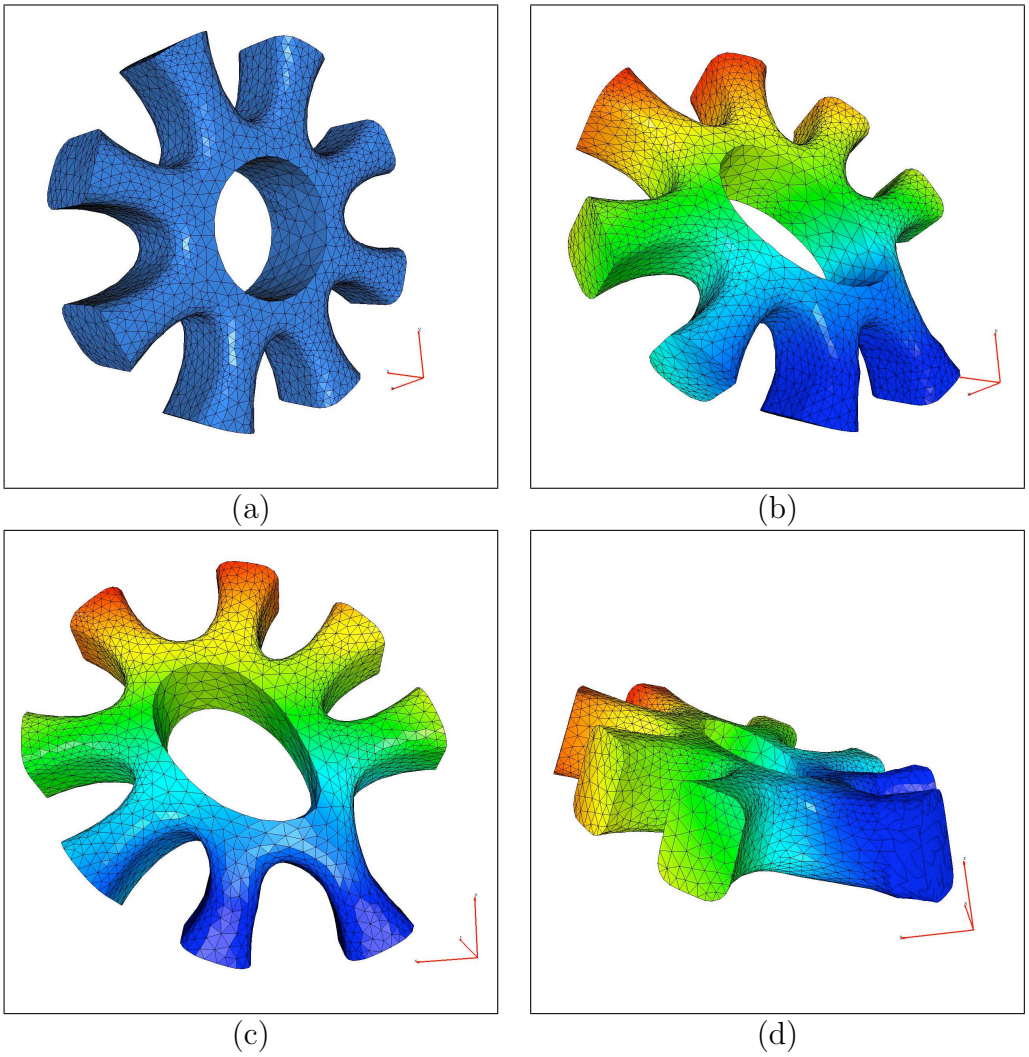

Figure 3: (a) Computational mesh, (b,c,d) Deformation of the mechanical device from various viewpoints.

3.2.1. Efficiency of the generalized formulation

As pointed out, our first objective is here to justify the choice of our mechanical model and to recover the relevant biophysical parameters. To this end, we compared the numerical results with experimental compressive tests on swine brain tissues obtained by [9]. In this test, the geometry of the domain is non relevant as the biophysical samples correspond to simple shapes with axisymmetric property.

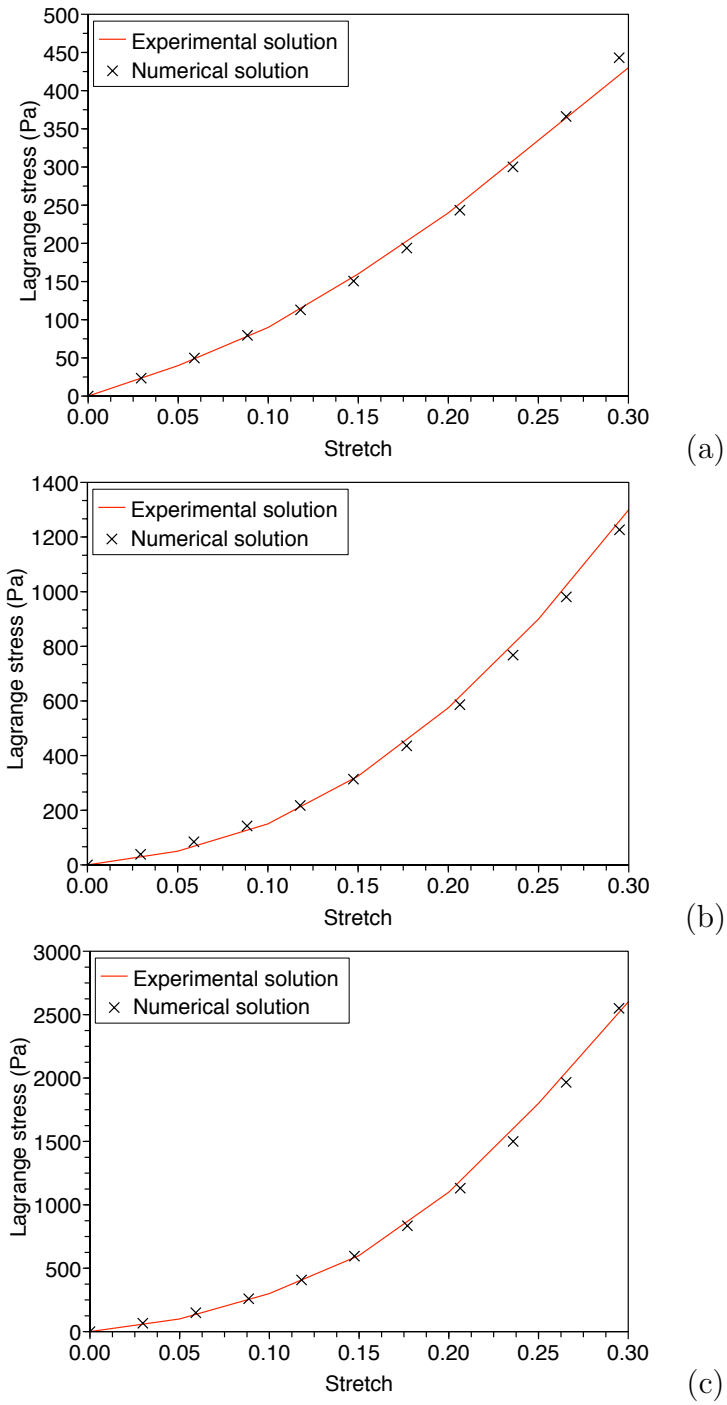

Figure 4: Evolution of the stress for three compression rates: (a) $6.4 \cdot 10^{-6}\, s^{-1}$, (b) $6.4 \cdot 10^{-3}\, s^{-1}$, (c) $6.4 \cdot 10^{-1}\, s^{-1}$. Comparison between the experimental solution reported by [9] and the numerical solution.

In order to reproduce the biophysical experiments, we needed to extend the energy functional introduced in (2) as follows:

$$\begin{aligned} W_0(C) &= \mathcal{C}_{01}(I_1(C) - 3) + \mathcal{C}_{02}(I_2(C) - 3), \\ W_i(y) &= \mathcal{C}_{i1}(y - 3) + \mathcal{C}_{i2}(y - 3)^2, \qquad \forall i \in \{1, 2\}. \end{aligned}$$

Figure 4 shows the comparison between the experimental and the numerical solutions corresponding to various compression rates. Table 2 reports the coefficients used to carry on these tests.

$\mathcal{C}_{01}$	$\mathcal{C}_{10}$	$\mathcal{C}_{11}$	$\mathcal{C}_{12}$	ν_1	$\mathcal{C}_{21}$	$\mathcal{C}_{22}$	ν_2
21	105	80	680	21500	150	2000	115

Table 2: Mechanical properties used for the test case

We observe that both curves are well in accordance with each other. This result clearly proves that our generalized model represents quite satisfactorily the biomechanical behavior of the brain structures under a compressive load and that the coefficients given in Table 2 are relevant for this study.

3.2.2. Description of the geometric model

Imaging and sensing devices are routinely used in biomedical applications to supply large datasets of voxels that define the contour of organs or biophysical domains. However, the latter need to be converted into conforming triangulations prior to be used in finite element procedures for solving a PDE problem like the one we are addressing here. This conversion stage is indeed important and often underestimated, as it aims at creating a triangulation that represents an accurate piecewise affine approximation of the geometry of the domain boundary with a minimal number of finite elements in the domain. Obviously, the triangulation procedure depends on the nature of data available, typically, a sequence of two-dimensional segmented images or a three-dimensional point cloud. In [3], we explained how to generate a surface triangulation based on various types of discrete data. Hence, we briefly review here the creation of a geometry dependent triangulation of the computational domain.

Suppose a conforming simplicial surface triangulation $\mathcal{S}_h$ is available, that provides a discrete representation of the domain geometry. At first, we analyze $\mathcal{S}_h$ in order to define a metric tensor field $M(x)$ at the mesh vertices of S_h that relates the local element size of any simplex $K \in \mathcal{S}_h$ to the local main

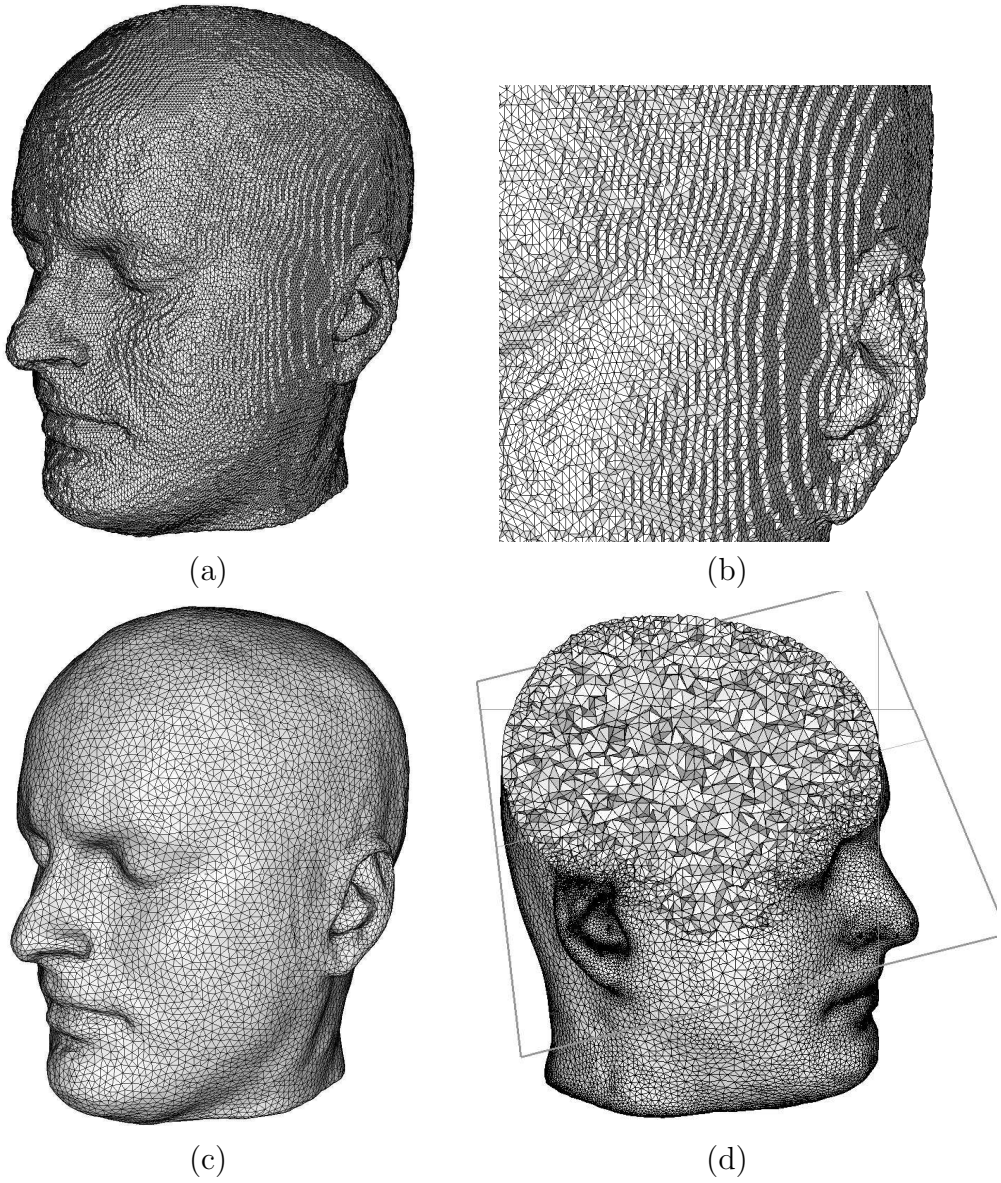

Figure 5: *(a,b) Surface triangulation obtained from MRI slices, (c) Surface triangulation adapted to the geometric properties, (d) Generation of a three-dimensional triangulation.*

curvatures and directions of curvature of the underlying surface defined by $\mathcal{S}_h$. This tensor is an efficient means to control the shape, the size as well as the orientation of mesh elements [4]. The next stage consists in generating

a surface triangulation in which all simplices have a unit size, *i.e.,* an excentricity ratio $\sigma = h/\rho$ (where h is the length of the longest edge and ρ is the radius of the inscribed sphere) controlled by the tensor $M(x)$. Figure 5 shows the result of the surface retriangulation procedure on a biomedical model of a human head. The next stage consists in creating a computational mesh $\mathcal{T}_h$ of the domain suitable for finite elements calculations. To this end, we rely on an efficient Delaunay point insertion procedure described in [4] that can be also used for adapting triangulations to any metric tensor given by an *a posteriori* error estimate.

3.3. Brain shift computation

To conclude, we provide a typical three dimensional result obtained by our approach, in the simulation of the numerical brain shift. The original data have been obtained using MR imaging devices. The bounding box of the domain corresponds to $15 \times 15 \times 15$ cm. The computational mesh contains $62,123$ vertices and $225,009$ tetrahedra. Figure 6 shows the results of the simulation for the values of the coefficients reported in Table 2 and corresponding to a gravity load $f = (0, 0, 20)\ N \cdot m^{-3}$ as can be found when the patient undergoes a change of position during the treatment. The maximum displacement observed is here 0.9 cm, well in accordance with the expected experimental result [8]. The inital volume is $1.1706 \cdot 10^3$ cm^3 and the final volume after deformation is $1.1705 \cdot 10^3$ cm^3.

4. Conclusions and perspectives

This analysis has clearly shown the ability of our generalized model to deal with complex problems, essentially in structural mechanics. However, for biomedical applications, it revealed the need to know biophysically meaningfull coefficients, *i.e.* coming from in vivo measurements, difficult to obtain in practice. To overcome this difficulty, we started to investigate a related inverse problem, in view of retrieving the biophysical coefficients in a fully non invasive manner [2]. As pointed out in the introduction, this model is intended to be coupled with a fluid model or a viscoplastic model, more appropriate to represent the complex behavior of the brain structure.

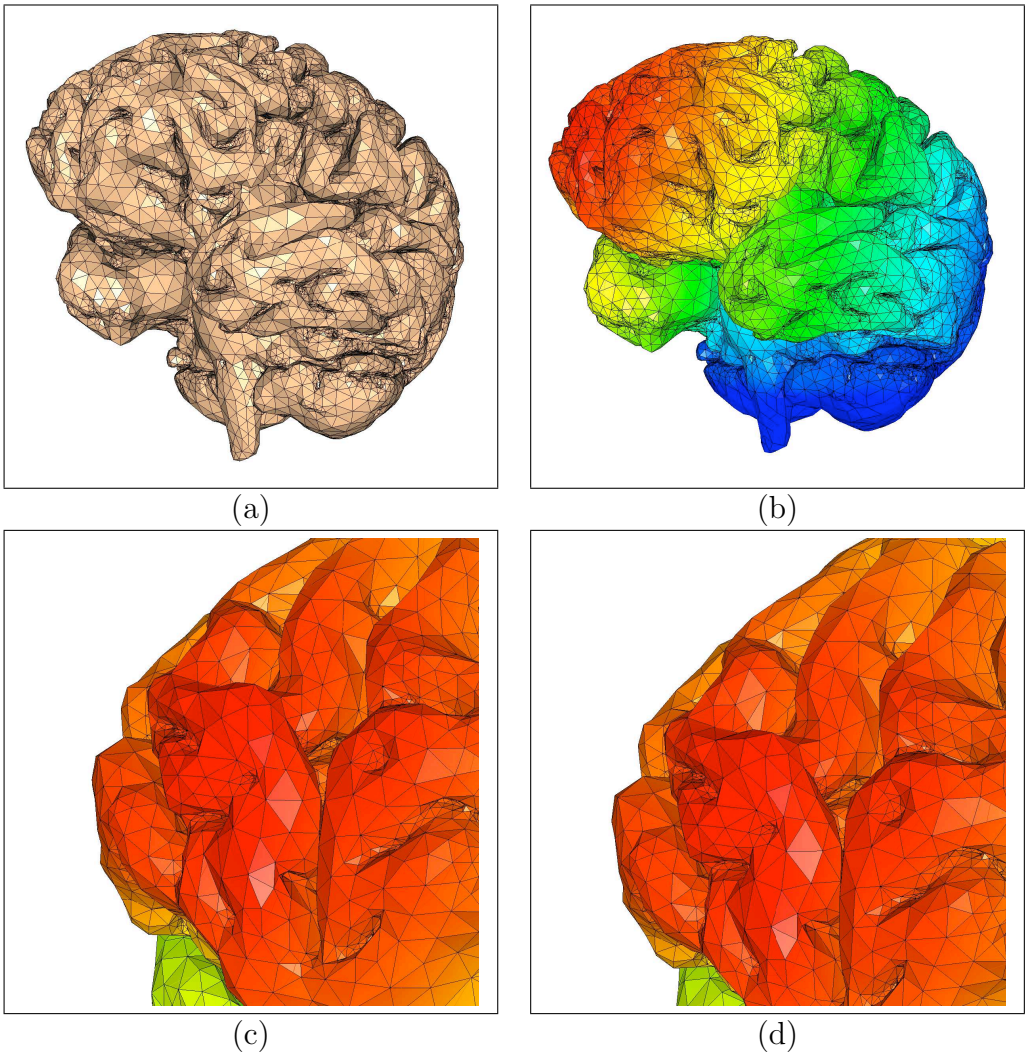

Figure 6: (a) Computational mesh, (b) Deformation field of the brain under gravity, (c) Local enlargment of the deformation field, (d) Displacement of the brain structure.

References

[1] Brands, D. W. A., Peters, G. W. M., Bovendeerd, P. H. M., 2004. Design and numerical implementation of a 3-D non-linear viscoelastic constitutive model for brain tissue during impact. Journal of Biomechanics 37, pp. 127-134.

[2] de Buhan, M., Osses, A., 2009. Logarithmic stability in determination

of a 3d viscoelastic coefficient and numerical examples. submitted.

[3] Frey, P., 2004. Generation and adaptation of computational surface meshes from discrete anatomical data. Int. J. Numer. Methods Eng. 60, pp. 1049-1074.

[4] Frey, P., George, P. L., 2008. Mesh generation. Application to finite elements, 2nd Edition. Wiley.

[5] le Tallec, P., 1994. Numerical methods for nonlinear three-dimensional elasticity. In: Handbook of Numerical Analysis. Vol. 3, pp. 465-624. P. G. Ciarlet and J.L. Lions eds, North-Holland.

[6] le Tallec, P., Rahier, C., Kaiss, A., 1993. Three-dimensional incompressible viscoelasticity in large strains: formulation and numerical approximation. Computer methods in applied mechanics and engineering 109, pp. 233-258.

[7] Lubliner, J., 1985. A model of rubber viscoelasticity. Mechanics Research Communications 12, pp. 93-99.

[8] Miga, M. I., Paulsen, K. D., Kennedy, F. E., Hoopes, P. J., Hartov, A., Roberts., D. W., 1998. Modeling surgical loads to account for subsurface tissue deformation during stereotactic surgery. IEEE SPIE Proceedings of Laser-Tissue Interaction IX, Part B: Soft-tissue Modeling 3254, pp. 501-511.

[9] Miller, K., 1997. Constitutive modelling of brain tissue : experiment and theory. Journal of Biomechanics 30, pp. 1115-1121.

[10] Miller, K., Chinzei, K., 2002. Mechanical properties of brain tissue in extension. Journal of Biomechanics 35, pp. 483-490.

[11] Nocedal, J., Wright, S. J., 1999. Numerical optimization. In: Springer Series in Operations Research. Springer.

[12] Oden, J. T., 1972. Finite Elements for Nonlinear Continua. McGraw Hill.

[13] Simo, J. C., 1987. On a fully three-dimensional finite-strain viscoelastic damage model: formulation and computational aspects. Computer methods in applied mechanics and engineering 60, pp. 153-173.